The pleckstrin-homology domain of dynamin is dispensable for membrane constriction and fission

Srishti Dar and Thomas J. Pucadyil*
Indian Institute of Science Education and Research, Pashan, Pune Maharashtra 411008, India

ABSTRACT **Classical dynamins bind the plasma membrane–localized phosphatidylinositol-4,5-bisphosphate using the pleckstrin-homology domain (PHD) and engage in rapid membrane fission during synaptic vesicle recycling. This domain is conspicuously absent among extant bacterial and mitochondrial dynamins, however, where loop regions manage membrane recruitment. Inspired by the core design of bacterial and mitochondrial dynamins, we reengineered the classical dynamin by replacing its PHD with a polyhistidine or polylysine linker. Remarkably, when recruited via chelator or anionic lipids, respectively, the reengineered dynamin displayed the capacity to constrict and sever membrane tubes. However, when analyzed at single-event resolution, the tube-severing process displayed long-lived, highly constricted prefission intermediates that contributed to 10-fold reduction in bulk rates of membrane fission. Our results indicate that the PHD acts as a catalyst in dynamin-induced membrane fission and rationalize its adoption to meet the physiologic requirement of a fast-acting membrane fission apparatus.**

Monitoring Editor
Patricía Bassereau
Institut Curie

Received: Sep 7, 2016
Revised: Oct 27, 2016
Accepted: Nov 3, 2016

INTRODUCTION

Membrane fission is governed by the general principle that a protein scaffold drives constriction of the underlying membrane, bringing them in close proximity, until they spontaneously fuse (Chernomordik and Kozlov, 2003). Because this process involves the formation of a narrow, neck-like intermediate, membrane fission is an energetically unfavorable process (Kozlovsky and Kozlov, 2003). Dynamin was the first protein shown to be directly involved in membrane fission (Koenig *et al.*, 1983; van der Bliek *et al.*, 1993). The dynamin superfamily of proteins is characterized by the presence of three conserved core domains: the GTPase (G)-domain, a bundle-signaling element (BSE), and the stalk (Chappie and Dyda, 2013). The G-domain binds and hydrolyzes GTP, the stalk maintains dynamin as a tetramer in solution and promotes dynamin self-assembly as helical scaffolds on the membrane, and the BSE acts as a toggle switch to stimulate its basal GTPase activity upon self-assembly (Faelber *et al.*, 2012). Dynamin1, the neuronal isoform of classical dynamins, functions to catalyze membrane fission during fast synaptic vesicle–recycling events (Schmid and Frolov, 2011). Unlike other members of the dynamin superfamily, which contain the characteristic core domains, classical dynamins are unique, as they possess a well-defined membrane binding, pleckstrin-homology domain (PHD) in the middle and a proline-arginine–rich domain (PRD) at the C-terminus. The PHD binds phosphatidylinositol-4,5-bisphosphate (PIP_2), whereas the PRD binds SH3 domain–containing endocytic accessory proteins (Okamoto *et al.*, 1997). Coincidence detection of the plasma membrane–localized PIP_2 and endocytic accessory proteins causes dynamin to be specifically recruited to emergent sites of membrane fission (Ferguson and De Camilli, 2012).

The importance of the PHD is underscored by the fact that mutations in centronuclear myopathy (CNM) and Charcot–Marie–Tooth (CMT) disease patients are predominantly located in this domain (Durieux *et al.*, 2010). Whereas CMT mutations affect lipid binding, CNM mutations map to a region on the PHD distant from those required for lipid binding (Kenniston and Lemmon, 2010). Considering that dynamin functions are critical for survival

This article was published online ahead of print in MBoC in Press (http://www.molbiolcell.org/cgi/doi/10.1091/mbc.E16-09-0640) on November 9, 2016.

*Address correspondence to: Thomas J. Pucadyil (pucadyil@iiserpune.ac.in).

Abbreviations used: BPLE, brain polar lipid extract; BSE, bundle-signaling element; CMT, Charcot–Marie–Tooth; CNM, centronuclear myopathy; DOPC, 1,2-dioleoyl-*sn*-glycero-3-phosphocholine; $DOPIP_2$, 1,2-dioleoyl-*sn*-glycero-3-phospho-(1′-myo-inositol-4′,5′ bisphosphate); DOPS, 1,2-dioleoyl-*sn*-glycero-3-phospho-L-serine; G-domain, GTPase domain; NTA, DGS NTA(Ni^{2+}); PHD, pleckstrin-homology domain; PRD, proline-arginine–rich domain; PIP_2, phosphatidylinositol-4,5-bisphosphate.

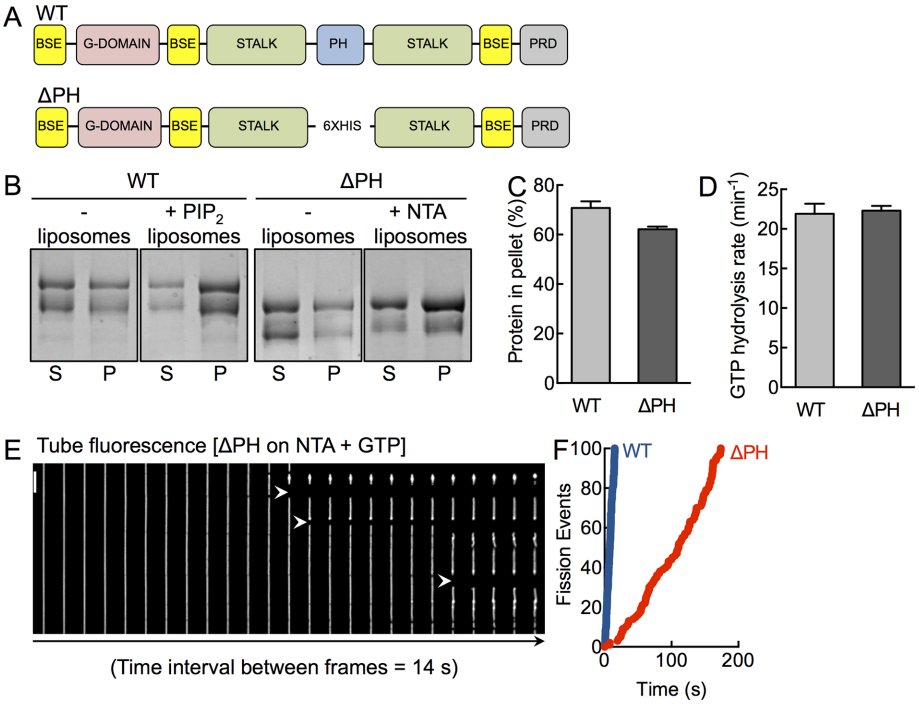

FIGURE 1: A functionally active dynamin construct lacking the PHD. (A) Schematic representation of dynamin showing the bundle-signaling element (BSE), GTPase domain (G-domain), stalk, pleckstrin-homology domain (PHD), and proline-arginine rich domain (PRD). The ΔPH construct has the entire PH domain deleted and replaced with a 6xHis linker. (B) Coomassie brilliant blue–stained SDS–PAGE of WT and ΔPH in the absence and presence of PIP_2- and NTA-containing liposomes after sedimentation, showing protein amounts in the supernatant (S) and pellet (P) fractions. The low–molecular weight band in both constructs reflects a proteolyzed form that partially lacks the C-terminus, which we confirmed using Western blotting with streptavidin-HRP, which binds the engineered StrepII tag at the C-terminus (Supplemental Figure S1). (C) Densitometric analysis of gels (both bands) shown in B, indicating the fraction of protein in the pellet. Data represent mean ± SD ($N = 2$). (D) Assembly-stimulated GTP hydrolysis rates of WT and ΔPH in presence of PIP_2- or NTA-containing liposomes, respectively. Data represent mean ± SD ($N = 3$). (E) Time-lapse sequence showing addition of ΔPH to SMrT templates in the presence of GTP. White arrowheads mark sites of scission. Scale bar, 5 μm. (F) Cumulative fission rates of WT (blue) and ΔPH (red). Data represent pooled analysis ($n \geq 19$, $N = 3$).

(Ferguson and De Camilli, 2012), their presence in surviving patients suggests that the PHD plays a subtle role in dynamin function. The functional relevance of the PHD in dynamin function is under debate. Early data from cells indicate that the partial or complete deletion of the PHD does not alter the subcellular localization of dynamin (Achiriloaie *et al.*, 1999; Vallis *et al.*, 1999), suggesting that the 109-residue globular domain plays more than a membrane-targeting role. The isolated PHD has very low affinity for anionic lipids, including PIP_2 (Klein *et al.*, 1998), but increases in avidity upon dynamin self-assembly. The crystal structure of the PHD identifies a β-sandwich core with three variable loops (VL1, VL2, and VL3), which together constitute the PIP_2-binding pocket (Lemmon and Ferguson, 2000). VL1 contains both hydrophobic and polar residues and partially inserts into the lipid bilayer (Ramachandran and Schmid, 2007). VL2 and VL3 are relatively polar in nature but are important for dynamin function, as evidenced by mutation studies (Liu *et al.*, 2011). In addition, recent studies point to a role of the PHD in negatively controlling dynamin self-assembly by binding to an autoinhibitory site on the stalk (Reubold *et al.*, 2015), an interface that is a hot spot for CNM mutations.

An active role for the PHD in dynamin function stems from observations that mutations disrupting the hydrophobicity of the VL1 loop tend to show reduced membrane remodeling and fission activity (Ramachandran *et al.*, 2009). Furthermore, theoretical considerations suggest a role for residues in this loop in splaying of lipids in the membrane in order to facilitate fission (Shnyrova *et al.*, 2013). Despite these observations, the specific role of the PHD in membrane fission has been difficult to interpret from mutagenesis approaches since the aforementioned mutations alter dynamics and orientation of the PHD on the membrane (Mehrotra *et al.*, 2014). Consequently, as discussed recently (Dar *et al.*, 2015), defects such as the inability to form stable scaffolds in the constant presence of GTP complicate any understanding of the direct role of the PHD in membrane fission.

RESULTS

A functionally active dynamin construct lacking the PHD

To specifically delineate the contribution of the PHD in dynamin function, we used an alternate approach of engineering a dynamin construct in which the 109-residue-long PHD is replaced by six histidine (His) residues. This construct, which we refer to as ΔPH (Figure 1A), can be recruited to membranes containing the chelator lipid DGS NTA(Ni^{2+}) (NTA; Kubalek *et al.*, 1994). Thus ΔPH allows us to monitor the consequences of a lack of PHD while still being recruited to the membrane. PolyHis-NTA interactions have been widely used to artificially recruit proteins to analyze a range of membrane-localized processes, such as Rab-effector interactions (Christis and Munro, 2012) and clathrin recruitment by adaptors (Kelly *et al.*, 2014), and to understand mechanisms of membrane curvature generation (Stachowiak *et al.*, 2012).

We first tested ΔPH in assays previously used to monitor dynamin function in vitro. ΔPH binds to and sediments with NTA-containing liposomes to levels comparable to that seen with wild type (WT) on PIP_2-containing liposomes (Figure 1, B and C). The low–molecular weight band in both constructs reflects a proteolyzed form that partially lacks the C-terminus, which we confirmed using Western blotting with streptavidin–horseradish peroxidase (HRP), which binds the engineered StrepII tag at the C-terminus (Supplemental Figure S1). The partially proteolyzed forms appear in the purified preparation likely because dynamin exists as a tetramer in solution. Dynamin self-assembles to form helical scaffolds on membranes, which in turn stimulates its basal GTP hydrolysis rates (Chappie *et al.*, 2010). Thus assembly-stimulated GTPase activity reflects proper orientation of the G-domains within the scaffold. We find that ΔPH has identical rates of lipid-stimulated GTPase activity on NTA-containing liposomes as seen with WT on PIP_2-containing liposomes (Figure 1D). Next we analyzed ΔPH for its ability to catalyze membrane fission in the presence of GTP on a recently described assay system of supported membrane tubes (SMrTs; Dar *et al.*, 2015). Remarkably, we find that the ΔPH severs membrane tubes (Figure 1E). These

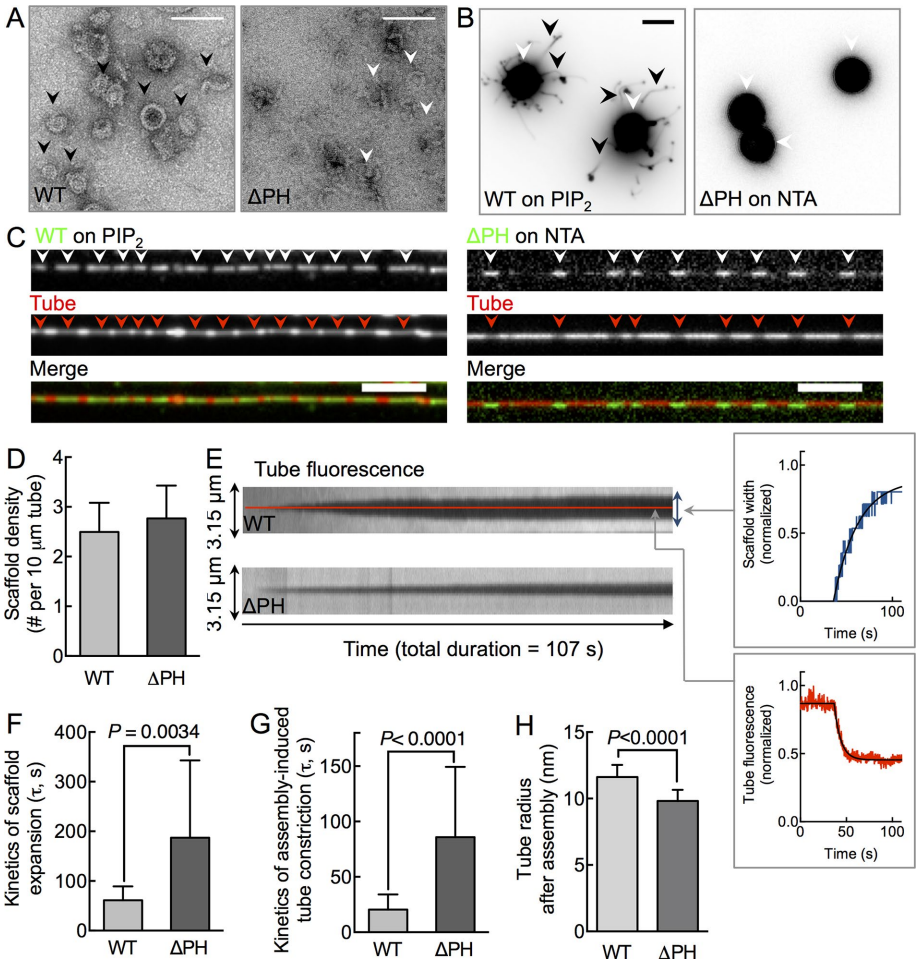

FIGURE 2: The PHD kinetically regulates dynamin self-assembly. (A) Representative negative-stained electron microscopy of WT and ΔPH in the presence of GMPPCP under low-salt conditions. Black arrowheads mark rings, and white arrowheads mark crescent-shaped, incomplete rings. Scale bar, 100 nm. (B) SUPER templates (white arrowheads) showing membrane tubules (black arrowheads) with WT but not ΔPH. Images are inverted in contrast for clarity. Scale bar, 5 μm. (C) Fluorescence micrographs showing the distribution of Alexa 488–labeled (green) WT and ΔPH on a *p*-Texas Red DHPE–labeled (red) membrane tube. White arrowheads mark dynamin scaffolds, and red arrowheads mark sites of tube constriction. Scale bars, 5 μm. (D) Scaffold density for WT and ΔPH. Data represent mean ± SD ($n = 3$, $N = 3$). (E) Kymographs of scaffold assembly–induced tube constriction for WT and ΔPH. Schematic of scaffold assembly–induced membrane tube constriction. Data are acquired in the tube fluorescence channel; the widening of the region of lower tube fluorescence (blue trace) indicates scaffold expansion, and the decay in fluorescence intensity (red trace) reflects assembly-induced tube constriction. (F) Time constant (τ) of scaffold expansion for WT and ΔPH. Data represent mean ± SD ($n \geq 20$, $N = 3$, Student's *t* test). (G) Time constant (τ) of scaffold assembly–induced tube constriction. Data represent mean ± SD ($n \geq 20$, $N = 3$, Student's *t* test). (H) Tube radius under scaffolds calculated according to Supplemental Figure S2. Data represent mean ± SD ($n \geq 21$, $N = 1$, Student's *t* test).

results indicate that the PHD is entirely dispensable for membrane fission. However, ΔPH was 10-fold slower than WT in cutting tubes (Figure 1F; fission $rate_{WT}$ = 6.7 cuts/s, fission $rate_{\Delta PH}$ = 0.6 cut/s; Supplemental Movie S1). We analyzed the molecular basis of the defect associated with ΔPH using stage-specific assays that monitor dynamin function at single-event resolution.

The PHD is a kinetic regulator of dynamin self-assembly

We first monitored ΔPH functions in a membrane-independent, dynamin self-assembly assay using negative-stain electron microscopy (Carr and Hinshaw, 1997). Incubation of WT with a nonhydrolyzable GTP analogue, GMPPCP, under low-salt conditions promotes dynamin self-assembly into rings or spirals (Figure 2A). Under similar conditions, ΔPH formed fewer assemblies, and those that formed appeared to be incomplete, crescent-shaped structures (Figure 2A). These results are in contrast to previous reports in which the removal of PHD was seen to promote dynamin self-assembly. We believe that these differences arise from the use of a full-length construct and deletion of the entire PHD in our case, as opposed to a full-length construct with partial deletion of the PHD (Achiriloaie *et al.*, 1999) or a construct lacking both the PHD and the PRD (Reubold *et al.*, 2015). Consistent with a defect in self-assembly in solution, ΔPH failed to remodel planar NTA-containing supported bilayers with excess membrane reservoir (SUPER) templates into long membrane tubes (Figure 2B), suggesting together that the PHD contributes to the cooperative self-association of dynamin molecules. Surprisingly, when added to SMrT templates and visualized after 10 min, fluorescently labeled ΔPH organized as discrete scaffolds (Figure 2C, white arrowheads). Moreover, as is seen with WT, ΔPH scaffolds constrict the underlying tube and reduce tube fluorescence (Figure 2C, red arrowheads), confirmed also by monitoring tube fluorescence of encapsulated monomeric enhanced green fluorescent protein (mEGFP; Supplemental Figure S2). Together these results suggest that a curved membrane rescues the self-assembly defect in ΔPH. Of importance, despite the membranes having different concentrations of the lipid that recruits WT and ΔPH to the membrane, the mean scaffold density seen with ΔPH was similar to that seen for WT (Figure 2D), suggesting that ΔPH is not compromised in membrane binding.

A closer look at the dynamics of scaffold formation revealed subtle defects associated with ΔPH. We assayed scaffold expansion and tube constriction from the drop in tube fluorescence under scaffolds (Figure 2C). Kymographs generated from time-lapse movies after dynamin addition to SMrT templates indicate that ΔPH scaffolds nucleate and laterally expand on the tube (Figure 2E, blue trace), similar to that seen for WT. However, analysis of multiple single events revealed significantly slower kinetics of scaffold expansion for ΔPH compared with that seen for WT (Figure 2F; $\tau_{WT} = 61 \pm 28$ s, mean ± SD, $n = 17$; $\tau_{\Delta PH} = 187 \pm 156$ s, mean ± SD, $n = 18$). As a control, hexahistidine (6xHis)-mEGFP is recruited to NTA-containing tubes with a τ of ~25 s, indicating that the slow kinetics of scaffold expansion seen with ΔPH is not due to reduced accessibility for NTA. Scaffold assembly led to a monotonous decay in tube fluorescence (Figure 2E, red trace), indicating tube constriction at the site of the growing scaffold for both WT and ΔPH. However, the kinetics

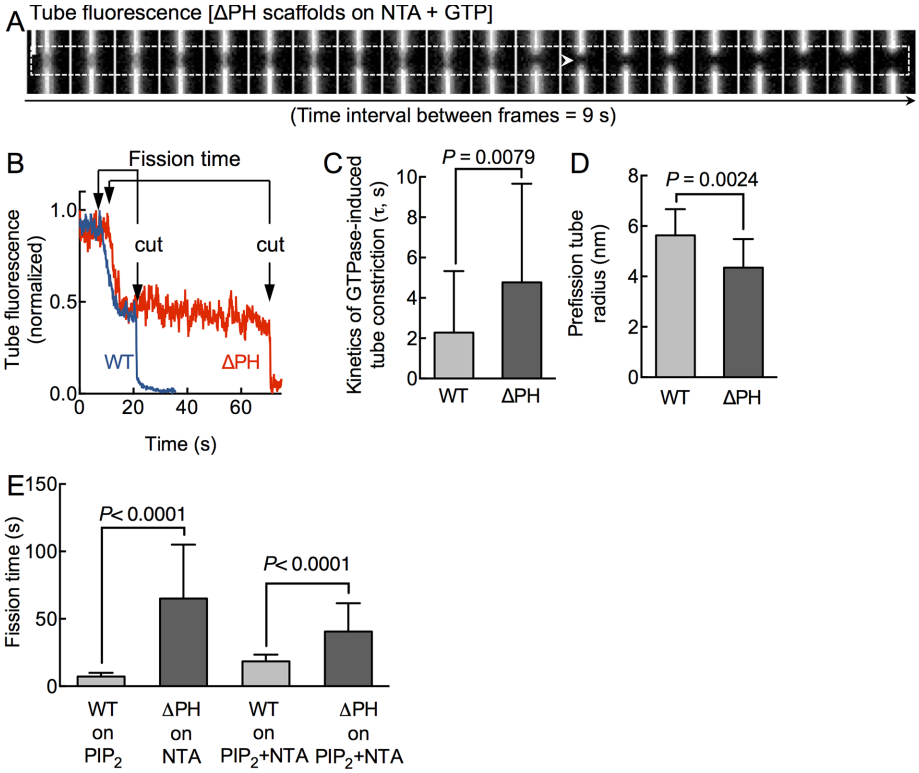

FIGURE 3: Catalytic role of the PHD in dynamin-induced membrane fission. (A) Time-lapse movie monitoring tube fluorescence changes under a ΔPH scaffold (dashed line) in response to GTP addition. White arrowhead marks site of scission. Scale bar, 5 μm. (B) Single-pixel tube fluorescence changes in response to GTP addition to WT (blue) and ΔPH (red) scaffolds. Fission time represents the time between onset of constriction and the cut in the tube. (C) Time constant (τ) of GTPase-induced tube constriction. Data represent mean ± SD ($n \geq 40$, $N = 3$, Student's *t* test). (D) Tube radius of the prefission intermediate calculated according to Supplemental Figure S2. Data represent mean ± SD ($n \geq 12$, $N = 1$, Student's *t* test). (E) Fission time of WT on PIP_2-containing (mean ± SD, $n = 82$, $N = 3$), ΔPH on NTA-containing ($n = 122$, $N = 3$), WT on PIP_2 + NTA–containing ($n = 14$, $N = 1$), and ΔPH on PIP_2 + NTA–containing ($n = 17$, $N = 1$) membranes. Significance analysis is carried out using Student's *t* test.

of assembly-induced tube constriction was fourfold slower for ΔPH than for WT (Figure 2G; $\tau_{WT} = 20 \pm 14$ s, mean ± SD, $n = 173$; $\tau_{\Delta PH} = 86 \pm 63$ s, mean ± SD, $n = 73$). Nevertheless, scaling pixel intensities to tube radii (Supplemental Figure S3) revealed that at equilibrium, ΔPH scaffolds appeared to constrict the underlying membrane tube to a radius of 9.8 ± 0.8 nm (mean ± SD, $n = 21$), slightly lower than the value of 11.6 ± 0.9 nm (mean ± SD, $n = 22$) for WT (Figure 2H). These results indicate that ΔPH is membrane active and highlight a role for the PHD in primarily facilitating the rate of dynamin assembly–induced membrane constriction.

The PHD catalyzes dynamin-induced membrane fission

Swapping the native PHD-PIP_2 interaction for a generic polyHis-NTA association preserves dynamin's ability to self-assemble on and constrict membrane tubes. This prompted us to monitor the effects of GTP addition to preassembled ΔPH scaffolds. Our earlier experiments with WT showed that the addition of GTP to preassembled scaffolds leads to further tube constriction, which is followed by tube scission (Dar *et al.*, 2015). Kinetics of GTPase-induced tube constriction provides specific insights into the mechanochemical attributes of dynamin. Of importance, fission time, defined as the time interval between the onset of tube constriction and the cut under a preassembled scaffold, indicates the actual catalytic efficiency of dynamin, since such an analysis overcomes complications arising from upstream membrane binding and assembly defects. GTP addition to preassembled ΔPH scaffolds led to tube constriction, followed by a cut (Figure 3A and Supplemental Movie S2). Single-pixel tube fluorescence traces acquired from under ΔPH (Figure 3B, red trace) and WT (Figure 3B, blue trace) scaffolds showed similar trends of GTPase-induced tube constriction before scission, with the important distinction that ΔPH fission events were characterized by a prolonged fission time. Analysis of multiple single tube scission events revealed that the kinetics of GTPase-induced tube constriction with ΔPH was only marginally slower than that seen with WT (Figure 3C; $\tau_{WT} = 2.3 \pm 3.0$ s, mean ± SD, $n = 44$; $\tau_{\Delta PH} = 4.7 \pm 4.8$ s, mean ± SD, $n = 39$). Again, scaling pixel intensities to tube radii (Supplemental Figure S3) revealed that ΔPH scaffolds use GTP hydrolysis to constrict the tube to ~4 nm radius before the cut, similar to that seen for WT (Figure 3D). Thus the mechanochemical coupling between GTPase-induced conformational changes in the scaffold and tube constriction is managed well even in the absence of a PHD. Remarkably, upon reaching these critical dimensions (~4-nm tube radius), ΔPH appeared to stall for variable time periods, whereas reactions with WT appeared to undergo near-spontaneous membrane scission. Consequently the fission time for ΔPH reactions shows a wide distribution centered about a mean value that is approximately ninefold higher than that seen with WT (Figure 3E; fission $time_{WT} = 7.2 \pm 2.7$ s, mean ± SD, $n = 82$; fission $time_{\Delta PH} = 65.0 \pm 40.0$ s, mean ± SD, $n = 122$). Taken together, the 10-fold-slower cutting rates seen with ΔPH (Figure 1F) are explained by slower rates of scaffold assembly and prolonged fission times. In addition to the kinetic delay in tube constriction, our results point to a role of the PHD that is downstream of coupling GTP hydrolysis to membrane constriction. We find that the PHD potently facilitates scission of a highly constricted prefission tube intermediate.

We arrived at the foregoing results by comparing fission activity of WT on PIP_2-containing membranes to ΔPH on NTA-containing membranes. A caveat in interpreting these results is the lack of control of lipid-specific effects to membrane fission. In other words, the effects we see with ΔPH can be attributed to the absence of the PHD, the presence of the NTA lipid used to recruit ΔPH, or both. To address this concern, we assayed fission time of WT and ΔPH on membranes containing both PIP_2 and NTA. We found that the presence of NTA increased WT fission time to 18.4 ± 5.0 s (Figure 3E; mean ± SD, $n = 14$), which is 2.6-fold higher than the value of 7.2 ± 2.8 s (mean ± SD, $n = 82$) for membranes lacking NTA. In addition, the presence of PIP_2 lowered ΔPH fission time to 40.5 ± 21.0 (mean ± SD, $n = 17$), which is 1.6-fold lower than the value of 65.0 ± 40.0 s (mean ± SD, $n = 122$) for membranes lacking PIP_2. Nevertheless, the absence of the PHD results in prolonging fission times (Figure 3E). Thus, although lipid-specific effects are significant, the lack of PHD clearly results in a delay in dynamin-catalyzed membrane fission.

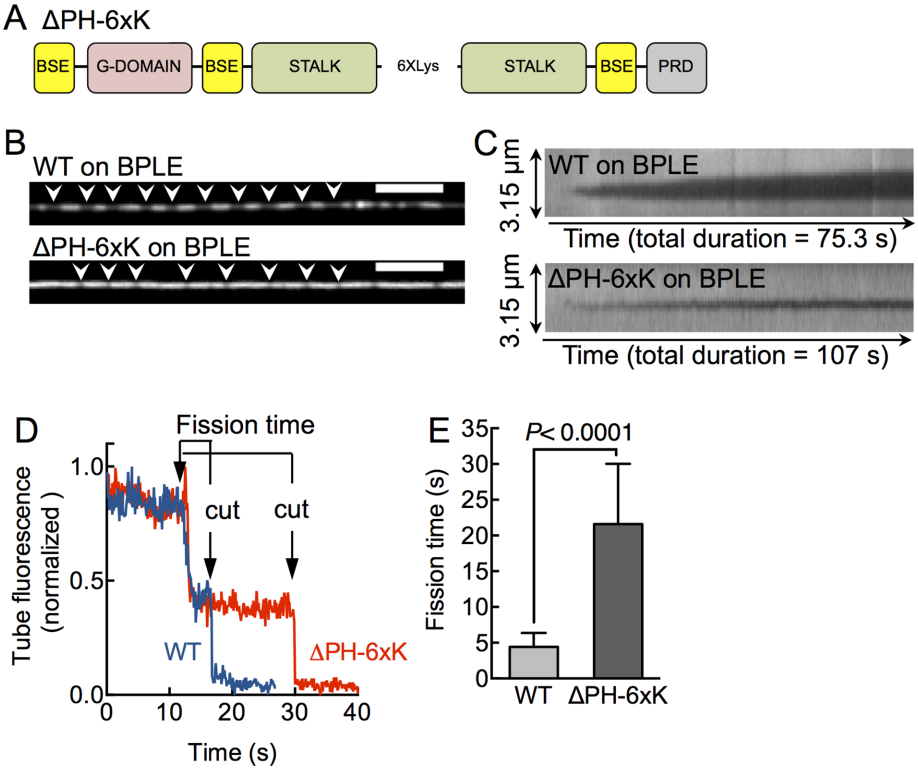

FIGURE 4: Effects with an alternate dynamin construct lacking the PHD on native membranes. (A) The ΔPH-6xK construct has the entire PH domain deleted and replaced with a 6xLys linker. (B) Fluorescence micrographs showing WT and ΔPH-6xK on a *p*-Texas Red DHPE–labeled membrane tube composed of BPLE. White arrowheads mark sites of tube constriction. Scale bars, 5 μm. (C) Kymographs of scaffold assembly–induced tube constriction for WT and ΔPH-6xK on BPLE. Data are acquired in the tube fluorescence channel, and the decay in fluorescence intensity reflects assembly-induced constriction of the tube underlying the scaffold. (D) Single-pixel tube fluorescence changes in response to GTP addition to WT (blue) and ΔPH-6xK (red) scaffolds on BPLE. Fission time represents time between onset of constriction and the cut in the tube. (E) Fission time for WT and ΔPH-6xK. Data represent mean ± SD ($n \geq 15$, $N = 1$, Student's *t* test).

To further address the specific contribution of the PHD in a more native setting and overcome lipid-specific effects, we engineered a second construct in which the PHD is replaced by six Lys residues (Figure 4A; ΔPH-6xK), which would facilitate a physiologically relevant, charge-based membrane recruitment, and compared its behavior to WT on a native-like membrane composed of brain polar lipid extract (BPLE). This extract was used earlier to reconstitute dynamin and effector recruitment to the membrane (Itoh *et al.*, 2005). Addition of 0.5 μM WT to SMrT templates with BPLE led to the formation of discrete scaffolds that constricted the underlying membrane tube (Figure 4B, white arrowheads). In contrast, ΔPH-6xK required much higher concentrations (10 μM) before scaffolds were apparent (Figure 4B, white arrowheads). ΔPH-6xK scaffolds were significantly shorter than WT scaffolds, signifying reduced affinity for the membrane. Indeed, kymographs generated from time-lapse movies indicate that ΔPH-6xK scaffolds nucleate and laterally expand at a slower rate on the tube compared with that seen for WT (Figure 4C). The diffraction-limited ΔPH-6xK scaffolds prevented us from further analyzing the extent of assembly-induced tube constriction. Nevertheless, GTP-addition to preassembled WT and ΔPH-6xK scaffolds on BPLE again led to tube constriction followed by cuts. Single-pixel tube fluorescence traces acquired from under ΔPH-6xK (Figure 4D, red trace) and WT (Figure 4D, blue trace) scaffolds showed similar trends of GTPase-induced tube constriction before scission, with the important distinction again that ΔPH-6xK fission events were characterized by a prolonged fission time. Analysis of multiple single tube scission events revealed that the fission time for ΔPH-6xK is approximately fivefold higher than with WT (Figure 4E; fission time_{WT} = 4.4 ± 1.9 s, mean ± SD, n = 75; fission $\text{time}_{\Delta PH\text{-}6xK}$ = 21.6 ± 8.4 s, mean ± SD, n = 15). Taken together, our results using two constructs lacking the PHD and recruited to the membrane by different mechanisms indicate a significant role of the PHD in facilitating scission of the highly constricted prefission tube intermediate.

Of note, our assays were carried out with synthetic lipids for which both the fatty acyl chains were dioleoyl derivatives, which are nonnative. We chose such synthetic lipids because of their low-phase transition temperatures, which would guarantee their existence in the fluid state under our assay temperature of 25°C. Furthermore, assays with such synthetic lipid mixtures allow the precise analysis of the contribution of individual lipids to the function studied—in this case, the contribution of the PH domain to membrane fission. The lipid composition of neuronal membranes where dynamin-1 acts is far more complex, however, and is abundant in polyunsaturated fatty acids (Pinot *et al.*, 2014). How relevant, then, are the parameters of dynamin-catalyzed membrane fission obtained using synthetic lipid mixtures to dynamin's function in vivo? To test this, we systematically compared fission times of preassembled WT scaffolds on membranes composed of three synthetic lipid mixtures with varying charge (1,2-dioleoyl-*sn*-glycero-3-phosphocholine [DOPC]:1,2-dioleoyl-*sn*-glycero-3-phospho-L-serine [DOPS]:1,2-dioleoyl-*sn*-glycero-3-phospho-(1′-myo-inositol-4′,5′ bisphosphate) [$DOPIP_2$] 84:15:1 mol%, DOPC:DOPS:$DOPIP_2$ 80:15:5 mol%, and DOPC:DOPS 60:40 mol%) to those seen on two native mixtures (Folch extract and BPLE; Supplemental Figure S4). Of importance, the fission times seen on native extracts are very similar to those seen with synthetic membranes, with less than twofold difference across all the mixtures studied. These differences are significantly smaller than the effects seen in the absence of the PHD reported in the present study. Furthermore, fission times seen with Folch extract and BPLE appear closer to that those on synthetic mixtures carrying high-charge DOPC:DOPS (60:40 mol%) and DOPC:DOPS:$DOPIP_2$ (80:15:5 mol%) membranes, suggesting that the net charge on the membrane contributes more than the acyl chain composition to the observed differences. Together our results validate the use of synthetic lipid mixtures to compare parameters of dynamin-catalyzed membrane fission.

Global determinants for efficient catalysis of membrane fission

Previous work indicated an important role for membrane insertion by VL1 in dynamin-induced membrane fission (Ramachandran and Schmid, 2007; Figure 5A). Using the suite of stage-specific fluorescence-based assays described here, we recently showed that the

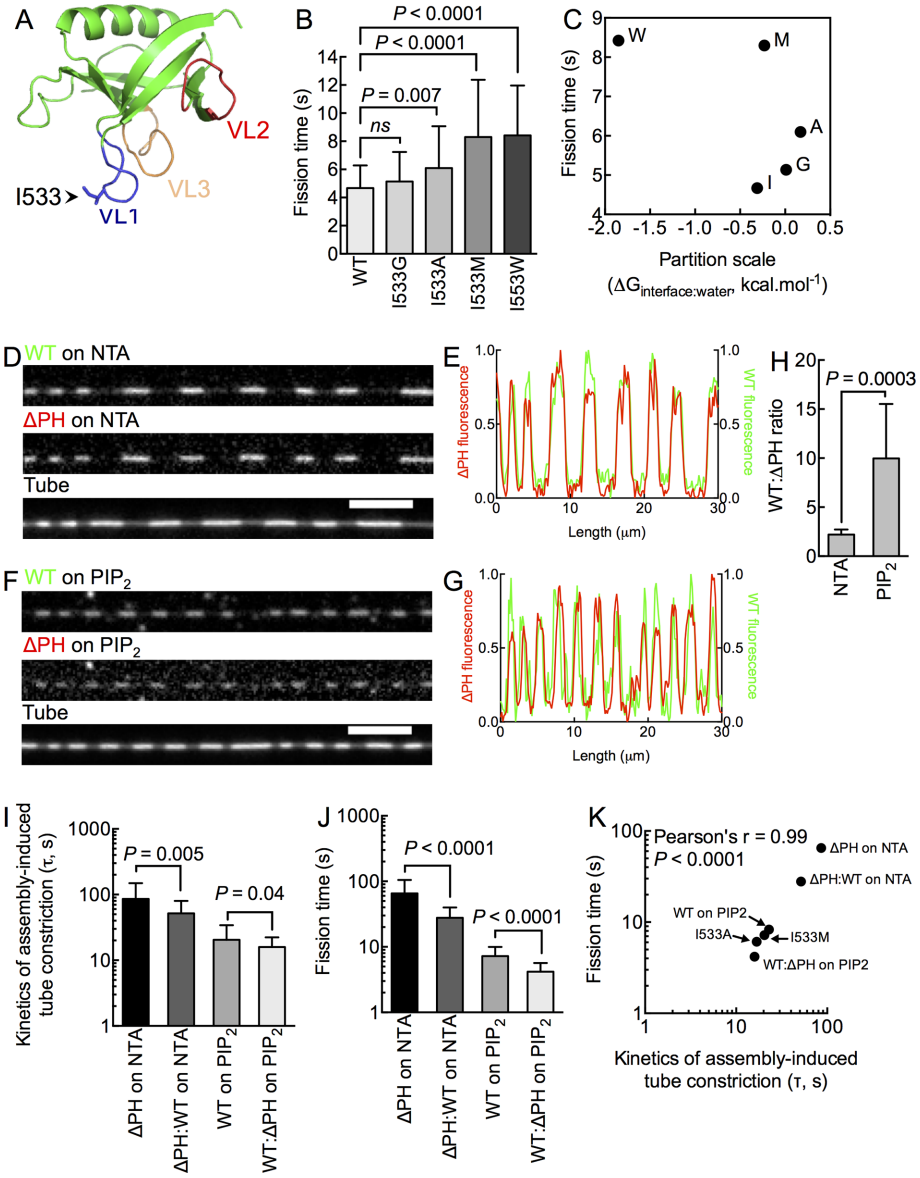

FIGURE 5: Determinants for efficient catalysis of membrane fission. (A) Structure of the dynamin1 PHD (Protein Data Bank code: 1DYN) indicating the position of VL1, 2, and 3 and the I533 residue at the tip of VL1. (B) Fission time for I533 substituted with different residues. Data represent mean ± SD ($n > 40$, $N = 3$, Student's t test). (C) Lack of correlation between residue hydrophobicity (Wimley and White scale) and fission time. Fluorescence micrographs (D, F) and line profiles (E, G) of Alexa 647–labeled WT (green) and Alexa 488–labeled ΔPH (red) scaffolds (white arrowheads) coassembled on NTA-containing (D) and PIP_2-containing (F) tubes. (H) WT:ΔPH fluorescence ratio on NTA- and PIP_2-containing tubes. Data represent mean ± SD ($n > 10$ scaffolds, $N = 1$, Student's t test). Time constants of scaffold assembly–induced tube constriction (I) and fission time (J) for pure (ΔPH or WT) and mixed (ΔPH:WT) scaffolds. Data represent mean ± SD ($n \geq 22$, $N = 3$, Student's t test). (K) Correlation between time constant (τ) of assembly-induced tube constriction and fission time.

cally significant, none of the mutants displayed a phenotype as severe as that seen with ΔPH (Figure 5B). Moreover, we found little correlation between residue hydrophobicity at the 533rd position to the fission time (Figure 5C). These results suggest contribution from additional residues in the PHD in catalyzing fission or an effect that can be ascribed to the entire PHD.

To test the latter possibility, we went back to assaying ΔPH on NTA membranes and asked whether defects associated with ΔPH scaffolds can be overcome by providing a PHD in-*trans*. For this, we added equimolar concentrations of ΔPH and WT to NTA-containing membrane tubes. Using orthogonally labeled ΔPH and WT constructs, we found WT to coassemble with ΔPH to form mixed scaffolds (Figure 5D). Thus WT fluorescence (green) strongly coincided with ΔPH fluorescence (red) (Figure 5E). Conversely, addition of equimolar concentrations of WT and ΔPH to PIP_2-containing membrane tubes also led to the formation of mixed scaffolds (Figure 5, F and G). The ratio of WT:ΔPH fluorescence was lower on NTA-containing tubes and higher on PIP_2-containing tubes (Figure 5H), which is consistent with the differences in scaffold assembly rates seen for each of these constructs (Figure 2F). Because scaffold assembly is attributed to proper alignment of the stalk regions (Faelber *et al.*, 2011; Ford *et al.*, 2011), the ability for ΔPH to coassemble with WT suggests that the ΔPH and WT are architecturally similar at the G-domain:stalk:BSE interface.

Mixed scaffolds on NTA-containing tubes displayed a significant enhancement in kinetics of assembly-induced tube constriction seen earlier with ΔPH alone (Figure 5I; $\tau_{\Delta PH} = 85.9 \pm 63.5$ s, mean ± SD, $n = 73$; $\tau_{\Delta PH:WT} = 51.6 \pm 28.3$ s, mean ± SD, $n = 11$). Surprisingly, mixed scaffolds on PIP_2-containing tubes also showed enhancement in kinetics of assembly-induced tube constriction seen earlier with WT (Figure 5I; $\tau_{WT} = 20.4 \pm 13.7$ s, mean ± SD, $n = 173$; $\tau_{\Delta PH:WT} = 15.9 \pm 6.4$ s, mean ± SD, $n = 13$). Next we added GTP to preassembled mixed scaffolds and monitored their response over time. Whereas the kinetics of GTPase-induced tube constriction showed marginal differences between mixed and pure scaffolds (Supplemental Figure S5), we found the fission time to be significantly affected. Thus mixed scaffolds on NTA-containing tubes showed fission times that were approximately twofold faster than that seen with ΔPH scaffolds, approaching estimates seen for WT on PIP_2-containing tubes (Figure 5J; fission $time_{\Delta PH} = 65.0 \pm 40.1$, mean ± SD, $n = 122$; fission $time_{\Delta PH:WT} = 27.9 \pm 12.7$, mean ± SD, $n = 43$). Thus organizing a PHD on a membrane lacking PIP_2 is sufficient to markedly improve the fission defect seen with ΔPH. Again surprisingly, mixed scaffolds on

primary defect associated with altering the hydrophobicity of VL1 by introducing the I533A mutation is an inability to form stable scaffolds in the constant presence of GTP (Dar *et al.*, 2015), which pertains to dynamin functions upstream of membrane fission per se. In fact, the fission defect with I533A can be overcome when it is preassembled on membrane tubes. To address comprehensively whether residues in VL1 indeed affect membrane fission, we substituted I533 with residues of varying hydrophobicity and tested them for fission times on preassembled scaffolds. To our surprise, although statisti-

PIP_2-containing tubes displayed fission times that were twofold faster than that seen with WT (Figure 5J; fission $time_{WT} = 7.2 \pm 2.7$, mean ± SD, $n = 82$; fission $time_{WT:\Delta PH} = 4.2 \pm 1.5$, mean ± SD, $n = 22$). Together these results lead us to conclude that mixed scaffolds display a gain of function in better catalyzing membrane fission. How can this be explained mechanistically? Combining our results on WT, ΔPH, mixed scaffolds, and the I533 mutants, we find that the fission time correlates quite well with kinetics of assembly-induced tube constriction (Figure 5K) rather than the kinetics of GTPase-induced tube constriction (Supplemental Figure S5), indicating that 1) the specific structural features of the PHD, as well as the global organization of multiple PHDs within the scaffold, influence the efficiency of the fission process, and 2) such contributions appear to be intrinsic to how the PHD interacts with or packs on the membrane rather than a GTP hydrolysis–dependent process.

DISCUSSION

Results from previous studies showing nucleotide-dependent changes to the average distance between the G-domain and the PHD in solution (Solomaha and Palfrey, 2005) and dissociation of scaffolds in response to GTP hydrolysis (Ramachandran and Schmid, 2007) were interpreted to reflect a functional coupling between the PHD and the G-domain. In addition, the origin of assembly-stimulated GTPase activity was interpreted to reflect a scenario in which the PHD transmits assembly-dependent conformational changes in the scaffold to the G-domain (Chappie *et al.*, 2010, 2011). If the PHD were specifically involved in such coupling, the ΔPH construct should have demonstrated effects in bulk rates of GTP hydrolysis and GTPase-induced tube constriction, which is not the case. Furthermore, scaffolds formed in the absence of the PHD constrict tubes to a similar extent as WT, indicating that the G-domain:stalk:BSE region is solely capable of transmitting conformational changes resulting from GTP hydrolysis to membrane constriction, thus explaining the evolutionary conservation of these domains among dynamins. The most striking defect in the absence of the PHD is the lingering presence of a prefission intermediate even after the tube has reached the critical dimension, which, from theory, is speculated to spontaneously lead to scission (Kozlovsky and Kozlov, 2003). Recent reports indicated that locking the G-domains in the transition state also results in a highly constricted tube intermediate (Mattila *et al.*, 2015). We believe it unlikely that the two intermediates are the same, since 1) the intermediate reported earlier emerges only when the GTPase cycle is stalled, whereas the one we find appears as the scaffold continues to hydrolyze GTP, 2) the intermediate we find stalls with variable efficiency, leading to a deregulated fission process, and 3) this intermediate manifests with mutants or constructs that also demonstrate an inability to efficiently manage a GTPase-independent membrane constriction, thereby rendering it a function not of dynamin's GTPase cycle, but of PHD–membrane interactions.

The long-lived prefission intermediate reveals the necessity for an additional energetic barrier to be overcome for tube scission. Previous work suggests partial disassembly and dissociation of dynamin scaffolds to contribute to the success of membrane fission (Ramachandran and Schmid, 2007; Bashkirov *et al.*, 2008; Pucadyil and Schmid, 2008). Although our recent work, monitoring how fluorescently labeled dynamin scaffolds behave during single membrane fission events, indicates that scaffold dissociation from the membrane is a process not central to tube scission (Dar *et al.*, 2015), a localized GTPase-induced scaffold disassembly process could be necessary for inducing rapid fission. Quite possibly, the strong interaction between ΔPH and NTA lipids could result in reduced off-rates of the scaffold from the membrane and contribute to prolonging the fission time. Perhaps the gain of function seen with mixed scaffolds reflects an effect by which the presence of dynamin molecules not directly engaged with the membrane facilitates GTPase-induced disassembly of the scaffold. Alternatively, given that the defect in the absence of the PHD manifests in highly variable fission times, we believe that the PHD catalyzes tube constriction and scission by exerting small, *kT*-level energy inputs to the underlying lipid bilayer. Given that the 109-residue-long PHD occupies a significant volume within the dynamin scaffold (Chappie *et al.*, 2011), we speculate that mixed scaffolds would cause the lipid bilayer to adopt a "corrugated" configuration. Perhaps the corrugated configuration facilitates transformation of a highly constricted tube to the hemifusion intermediate, as suggested in recent coarse-grained simulations (Fuhrmans and Müller, 2015), and could explain the gain of function seen in mixed scaffolds. We speculate that the greater the amplitude of such corrugations, the faster would be the progress of tube constriction and fission reactions. Thus scaffolds comprising ΔPH would produce the smallest degree of such undulations, followed by WT and mixed scaffolds, in that order.

Our results from monitoring partial reactions leading to membrane fission indicate the PHD to be dispensable for membrane fission. The consequence, however, is a sluggish scaffold assembly and membrane fission reaction. Our results help in understanding the influence of the PHD in the spatiotemporal regulation of discrete stages of dynamin function. Thus the PHD acts by enhancing cooperativity between dynamin subunits, thereby allowing the rapid formation of scaffolds that constrict the necks of emergent vesicles. After this, the PHD aids in the rapid formation of a possible hemifused intermediate, causing the neck to undergo scission. From an evolutionary standpoint, the PHD appears to be a recent addition in classical dynamins. In fact, functions of membrane binding appear to be managed by loop regions among the bacterial and mitochondrial dynamins. Thus the physiological requirement for a fast-acting membrane fission apparatus appears to have been fulfilled by the adoption of the PHD by the classical dynamins.

MATERIALS AND METHODS

Expression, purification, and fluorescence labeling of proteins

Full-length human dynamin1 (WT) was cloned with a C-terminal StrepII tag in pET15B vector. Residues 520–629, corresponding to the PHD, were deleted and replaced with 6xHis and/or 6xLys to generate the ΔPH and ΔPH-6xK constructs, respectively. All clones were confirmed by sequencing. Proteins were expressed in BL21(DE3) in autoinduction medium (Formedium, United Kingdom) at 18°C for 30 h and purified as described previously (Dar *et al.*, 2015). Purified proteins were labeled with extrinsic, cysteine-reactive Alexa 488 C5 or Alexa 647 C5 maleimide fluorescent probes (Invitrogen, Carlsbad, CA) as described previously (Dar *et al.*, 2015).

Preparation of liposomes and SUPER and SMrT templates

BPLE (141101; Avanti Polar Lipids, Alabaster, AL) or Folch lipids (B1502; Sigma Aldrich, St. Louis, MO) were used as is. Lipid stocks (Avanti Polar Lipids) were aliquoted in the following proportions to generate PIP_2-, NTA-, or PIP_2 plus NTA–containing mixtures: DOPC:DOPS:$DOPIP_2$ (84:15:1 mol%), DOPC:DOPS:NTA (80:15:5 mol%), and DOPC:DOPS:$DOPIP_2$:NTA (79:15:1:5 mol%). When necessary, trace amounts of the fluorescent lipid probe *p*-Texas Red 1,2-dihexadecanoyl-sn-glycero-3-phosphoethanolamine, triethylammonium salt (DHPE) was incorporated to a final

concentration of 1 mol%. For liposomes, dried lipid mixtures were hydrated in assay buffer (20 mM 4-(2-hydroxyethyl)-1-piperazineethanesulfonic acid [HEPES], pH 7.5, 150 mM KCl) to a final concentration of 1 mM and extruded through 100-nm polycarbonate membranes (Avanti Polar Lipids). SUPER templates were prepared with PIP_2- or NTA-containing liposomes as previously reported (Pucadyil and Schmid, 2010). SMrT templates were prepared as described previously (Dar *et al.*, 2015, 2017).

Liposome binding assays

WT or ΔPH at a final concentration of 1 μM was incubated with 100 μM PIP_2- and NTA-containing liposomes, respectively, for 30 min at room temperature in assay buffer. The liposome-bound (pellet [P]) and free (supernatant [S]) protein fractions were separated by high-speed (100,000 × *g*) centrifugation. Samples were resolved on a 10% SDS–PAGE and stained with Coomassie brilliant blue.

GTPase assay

WT or ΔPH at a final concentration of 0.1 μM was incubated with 10 μM PIP_2- or NTA-containing liposomes, respectively, in assay buffer containing 1 mM GTP (Jena Bioscience, Germany) and 1 mM $MgCl_2$ for 30 min at 37°C. GTP hydrolysis was monitored over time using a malachite green–based colorimetric assay (Baykov *et al.*, 1988).

SUPER template tubulation assays

Glass-bottomed Lab-Tek (Nalgene-Nunc, Rochester, NY) chambers were passivated with 2 mg/ml bovine serum albumin (Sigma-Aldrich) and filled with 200 μl of assay buffer containing 2 μM WT or ΔPH. A small aliquot (20 μl) of the stock of SUPER templates was added to the chamber, incubated for 10 min at room temperature, and imaged as described in what follows.

Electron microscopy

WT or ΔPH at a final concentration of 4 μM was incubated with 1 mM GMPPCP (Jena Bioscience, Germany) and 1 mM $MgCl_2$ in low-salt assay buffer (20 mM HEPES, pH 7.5, 35 mM NaCl) for 2 h at room temperature. The mixture was then adsorbed onto carbon-coated grids, stained with 1% uranyl acetate, and imaged with a 200-keV electron microscope.

SMrT template assays

SMrT templates assays to monitor scaffold assembly and membrane fission were carried out as 25°C as described previously (Dar *et al.*, 2015).

Fluorescence microscopy

Fluorescence imaging was carried out on an Olympus IX71 inverted microscope through a 100×, 1.4 numerical aperture oil-immersion objective equipped with an Evolve 512 electron-multiplying charge-coupled device camera (Photometrics, Tucson, AZ).

Statistical analysis

All nonlinear regression analyses were carried out using GraphPad Prism (version 5.0a). Where mentioned, *n* and *N* refer to the number of membrane tubes sampled and the number of independent experiments, respectively.

Image analysis and conversion of tube fluorescence to radius

Image analysis of fluorescence micrographs and time-lapse movies were carried out using Fiji (version 1.47; Schindelin *et al.*, 2012) The membrane tubes were labeled with the fluorescent lipid probe *p*-Texas Red DHPE, which partitions equally to regions of low and high membrane curvature (Hsieh *et al.*, 2012), exhibits fluorescence properties that are insensitive to protein binding (Jung *et al.*, 2009), and displays unrestricted diffusion in membrane tubes (Dar *et al.*, 2015). Scaffold expansion rates were analyzed by converting scaffold assembly kymographs into a binary image (after appropriate thresholding) and plotting the mean fluorescence intensity with time. Scaffold assembly–induced tube constriction rates were analyzed by acquiring a profile of a line placed at the middle of a kymograph showing a growing scaffold and plotting the change in fluorescence intensity with time. Kinetics in both these cases is calculated by fitting the plots to a plateau followed by a one-phase exponential decay equation. To validate whether the drop in tube fluorescence upon scaffold assembly indeed reflects tube constriction, we prepared SMrT templates doped with 5 mol% NTA in assay buffer containing 1 μM purified 6xHis-mEGFP. This led to binding of mEGFP to the outer and inner monolayers of membrane tubes. mEGFP bound to the outer monolayer was then stripped by passing assay buffer containing 100 mM EDTA. Conversion of tube fluorescence to radius was carried out using the supported lipid bilayer (SLB) formed at the source of SMrT template preparations as an in situ calibration standard (Supplemental Figure S3A; also see Dar *et al.*, 2017). This conversion is based on the premise that the fluorescence intensity of diffraction-limited, membrane-bound objects is proportional to the net membrane area (Kunding *et al.*, 2008). Before each experiment, fluorescence micrographs of the SLB and tubes were acquired and corrected for background. The integrated fluorescence intensity of regions of interest (ROIs) of different sizes placed on the SLB (Supplemental Figure S3B) was plotted against their respective area to get the calibration constant K_1 (Supplemental Figure S3C). The integrated fluorescence of ROIs of length l placed on tubes (Supplemental Figure S3D) was then converted into net membrane area using K_1, after which the radius r of the tube was calculated from $r = \text{area}/(2\pi l)$. The estimated tube radius r was then plotted against the maximum pixel intensity in ROIs placed on tubes to get the calibration constant K_2 (Supplemental Figure S3E). Tube fluorescence can then directly be converted into tube radius by dividing pixel intensities in a micrograph with K_2. Errors arising from fluctuations in tube fluorescence in still micrographs or time-lapse movies of tubes account for <10% coefficient of variation of mean fluorescence (Supplemental Figure S3F). We validated this approach by estimating the tube radius under a dynamin scaffold. A kymograph of a 10-s movie of a preassembled dynamin scaffold was first acquired (Supplemental Figure S3G). All pixels in the kymograph were converted into tube radius by dividing their intensity by K_2. A histogram of tube radii was then fitted to a sum of two Gaussians (Supplemental Figure S3H). The low-value peak, corresponding to the tube radius under the scaffold, gave an estimate of 7.9 ± 0.6 nm (mean ± SD, $n = 15$; Supplemental Figure S3I). These estimates reflect the tube radius from the center of the lumen to the center of the bilayer. Addition of 2.5 nm to this estimate to account for the 5-nm-thick lipid bilayer brings the tube radius under a dynamin scaffold to 10.4 nm, in good agreement with the value of 11.2 nm reported from force spectroscopy (Roux *et al.*, 2010).

ACKNOWLEDGMENTS

We thank Manidipa Banerjee, Mohit Kumar, and Riti Rawat for help with electron microscopy and Raunaq Deo for help with Western blots used to probe the proteolysis of dynamin constructs. We thank

members of the Pucadyil laboratory for comments on the manuscript. S.D. acknowledges the Council for Scientific and Industrial Research for a Senior Research Fellowship. T.J.P. acknowledges the Wellcome Trust-DBT India Alliance and the Indian Institute of Science Education and Research Pune for research funds. T.J.P. was an Intermediate Fellow of the Wellcome Trust-DBT India Alliance.

REFERENCES

Achiriloaie M, Barylko B, Albanesi JP (1999). Essential role of the dynamin pleckstrin homology domain in receptor-mediated endocytosis. Mol Cell Biol 19, 1410–1415.

Bashkirov PV, Akimov SA, Evseev AI, Schmid SL, Zimmerberg J, Frolov VA (2008). GTPase cycle of dynamin is coupled to membrane squeeze and release, leading to spontaneous fission. Cell 135, 1276–1286.

Baykov AA, Evtushenko OA, Avaeva SM (1988). A malachite green procedure for orthophosphate determination and its use in alkaline phosphatase-based enzyme immunoassay. Anal Biochem 171, 266–270.

Carr JF, Hinshaw JE (1997). Dynamin assembles into spirals under physiological salt conditions upon the addition of GDP and gamma-phosphate analogues. J Biol Chem 272, 28030–28035.

Chappie JS, Acharya S, Leonard M, Schmid SL, Dyda F (2010). G domain dimerization controls dynamin's assembly-stimulated GTPase activity. Nature 465, 435–440.

Chappie JS, Dyda F (2013). Building a fission machine–structural insights into dynamin assembly and activation. J Cell Sci 126, 2773–2784.

Chappie JS, Mears JA, Fang S, Leonard M, Schmid SL, Milligan RA, Hinshaw JE, Dyda F (2011). A pseudoatomic model of the dynamin polymer identifies a hydrolysis-dependent powerstroke. Cell 147, 209–222.

Chernomordik LV, Kozlov MM (2003). Protein-lipid interplay in fusion and fission of biological membranes. Annu Rev Biochem 72, 175–207.

Christis C, Munro S (2012). The small G protein Arl1 directs the trans-Golgi-specific targeting of the Arf1 exchange factors BIG1 and BIG2. J Cell Biol 196, 327–335.

Dar S, Kamerkar SC, Pucadyil TJ (2015). A high-throughput platform for real-time analysis of membrane fission reactions reveals dynamin function. Nat Cell Biol 17, 1588–1596.

Dar S, Kamerkar SC, Pucadyil TJ (2017). Using the supported membrane tubes (SMrT) assay system for real-time analysis of membrane fission reactions. Nat Protoc (*in press*).

Durieux A-C, Prudhon B, Guicheney P, Bitoun M (2010). Dynamin 2 and human diseases. J Mol Med 88, 339–350.

Faelber K, Held M, Gao S, Posor Y, Haucke V, Noé F, Daumke O (2012). Structural insights into dynamin-mediated membrane fission. Structure 20, 1621–1628.

Faelber K, Posor Y, Gao S, Held M, Roske Y, Schulze D, Haucke V, Noé F, Daumke O (2011). Crystal structure of nucleotide-free dynamin. Nature 477, 556–560.

Ferguson SM, De Camilli P (2012). Dynamin, a membrane-remodelling GTPase. Nat Rev Mol Cell Biol 13, 75–88.

Ford MGJ, Jenni S, Nunnari J (2011). The crystal structure of dynamin. Nature 477, 561–566.

Fuhrmans M, Müller M (2015). Coarse-grained simulation of dynamin-mediated fission. Soft Matter 11, 1464–1480.

Hsieh W-T, Hsu C-J, Capraro BR, Wu T, Chen C-M, Yang S, Baumgart T (2012). Curvature sorting of peripheral proteins on solid-supported wavy membranes. Langmuir 28, 12838–12843.

Itoh T, Erdmann KS, Roux A, Habermann B, Werner H, De Camilli P (2005). Dynamin and the actin cytoskeleton cooperatively regulate plasma membrane invagination by BAR and F-BAR proteins. Dev Cell 9, 791–804.

Jung H, Robison AD, Cremer PS (2009). Detecting protein–ligand binding on supported bilayers by local pH modulation. J Am Chem Soc 131, 1006–1014.

Kelly BT, Graham SC, Liska N, Dannhauser PN, Honing S, Ungewickell EJ, Owen DJ (2014). AP2 controls clathrin polymerization with a membrane-activated switch. Science 345, 459–463.

Kenniston JA, Lemmon MA (2010). Dynamin GTPase regulation is altered by PH domain mutations found in centronuclear myopathy patients. EMBO J 29, 3054–3067.

Klein DE, Lee A, Frank DW, Marks MS (1998). The pleckstrin homology domains of dynamin isoforms require oligomerization for high affinity phosphoinositide binding. J Biol Chem 273, 27725–27733.

Koenig J, Saito K, Ikeda K (1983). Reversible control of synaptic transmission in a single gene mutant of Drosophila melanogaster. J Cell Biol 96, 1517–1522.

Kozlovsky Y, Kozlov MM (2003). Membrane fission: model for intermediate structures. Biophys J 85, 85–96.

Kubalek EW, Le Grice SFJ, Brown PO (1994). Two-dimensional crystallization of histidine-tagged, HIV-1 reverse transcriptase promoted by a novel nickel-chelating lipid. J Struct Biol 113, 117–123.

Kunding AH, Mortensen MW, Christensen SM, Stamou D (2008). A fluorescence-based technique to construct size distributions from single-object measurements: application to the extrusion of lipid vesicles. Biophys J 95, 1176–1188.

Lemmon MA, Ferguson KM (2000). Signal-dependent membrane targeting by pleckstrin homology (PH) domains. Biochem J 350, 1–18.

Liu YW, Neumann S, Ramachandran R, Ferguson SM, Pucadyil TJ, Schmid SL (2011). Differential curvature sensing and generating activities of dynamin isoforms provide opportunities for tissue-specific regulation. Proc Natl Acad Sci USA 108, E234–E242.

Mattila J-P, Shnyrova AV, Sundborger AC, Hortelano ER, Fuhrmans M, Neumann S, Müller M, Hinshaw JE, Schmid SL, Frolov VA (2015). A hemi-fission intermediate links two mechanistically distinct stages of membrane fission. Nature 524, 109–113.

Mehrotra N, Nichols J, Ramachandran R (2014). Alternate pleckstrin homology domain orientations regulate dynamin-catalyzed membrane fission. Mol Biol Cell 25, 879–890.

Okamoto PM, Herskovits JS, Vallee RB (1997). Role of the basic, proline-rich region of dynamin in Src homology 3 domain binding and endocytosis. J Biol Chem 272, 11629–11635.

Pinot M, Vanni S, Pagnotta S, Lacas-Gervais S, Payet LA, Ferreira T, Gautier R, Goud B, Antonny B, Barelli H (2014). Polyunsaturated phospholipids facilitate membrane deformation and fission by endocytic proteins. Science 345, 693–697.

Pucadyil TJ, Schmid SL (2008). Real-time visualization of dynamin-catalyzed membrane fission and vesicle release. Cell 135, 1263–1275.

Pucadyil TJ, Schmid SL (2010). Supported bilayers with excess membrane reservoir: a template for reconstituting membrane budding and fission. Biophys J 99, 517–525.

Ramachandran R, Pucadyil TJ, Liu Y-W, Acharya S, Leonard M, Lukiyanchuk V, Schmid SL (2009). Suppl. Membrane insertion of the pleckstrin homology domain variable loop 1 is critical for dynamin-catalyzed vesicle scission. Mol Biol Cell 20, 4630–4639.

Ramachandran R, Schmid SL (2007). Real-time detection reveals that effectors couple dynamin's GTP-dependent conformational changes to the membrane. EMBO J 27, 27–37.

Reubold TF, Faelber K, Plattner N, Posor Y, Ketel K, Curth U, Schlegel J, Anand R, Manstein DJ, Noe F, *et al.* (2015). Crystal structure of the dynamin tetramer. Nature 525, 404–408.

Roux A, Koster G, Lenz M, Sorre B, Manneville J-B, Nassoy P, Bassereau P (2010). Membrane curvature controls dynamin polymerization. Proc Natl Acad Sci USA 107, 4141–4146.

Schindelin J, Arganda-Carreras I, Frise E, Kaynig V, Longair M, Pietzsch T, Preibisch S, Rueden C, Saalfeld S, Schmid B, *et al.* (2012). Fiji: an open-source platform for biological-image analysis. Nat Methods 9, 676–682.

Schmid SL, Frolov VA (2011). Dynamin: functional design of a membrane fission catalyst. Annu Rev Cell Dev Biol 27, 79–105.

Shnyrova AV, Bashkirov PV, Akimov SA, Pucadyil TJ, Zimmerberg J, Schmid SL, Frolov VA (2013). Geometric catalysis of membrane fission driven by flexible dynamin rings. Science 339, 1433–1436.

Solomaha E, Palfrey HC (2005). Conformational changes in dynamin on GTP binding and oligomerization reported by intrinsic and extrinsic fluorescence. Biochem J 391, 601.

Stachowiak JC, Schmid EM, Ryan CJ, Ann HS, Sasaki DY, Sherman MB, Geissler PL, Fletcher DA, Hayden CC (2012). Membrane bending by protein–protein crowding. Nat Cell Biol 14, 944–949.

Vallis Y, Wigge P, Marks B, Evans PR, McMahon HT (1999). Importance of the pleckstrin homology domain of dynamin in clathrin-mediated endocytosis. Curr Biol 9, 257–260.

van der Bliek AM, Redelmeier TE, Damke H, Tisdale EJ, Meyerowitz EM, Schmid SL (1993). Mutations in human dynamin block an intermediate stage in coated vesicle formation. J Cell Biol 122, 553–563.